bioRxiv preprint doi: https://doi.org/10.1101/2022.08.23.503752; this version posted August 25, 2022. The copyright holder for this preprint (which was not certified by peer review) is the author/funder, who has granted bioRxiv a license to display the preprint in perpetuity. It is made available under aCC-BY-NC 4.0 International license.

A robust backscatter modulation scheme for uninterrupted ultrasonic powering and back-communication of deep implants

Lukas Holzapfel[1] and Vasiliki Giagka[1, 2]

[1]Fraunhofer Institute for Reliability and Microintegration IZM, Berlin, Germany
[2]Delft University of Technology, Delft, The Netherlands

August 23, 2022

1 Abstract

Traditionally, active implants are powered by batteries, which, when discharged, have to be either replaced or recharged by an inductive power link. In the recent years, ultrasonic power links are also being investigated, as they promise more available power for deeply implanted miniaturized devices. Such devices often need to transfer information back, for example sensor data or some status information of the implant. For ultrasonically powered implants, this data transfer is usually achieved with On-Off Keying (OOK) based on load or backscatter modulation, or active driving of a secondary transducer.

In this paper, we propose to superimpose OOK with subcarriers, effectively leveraging Frequency-Shift Keying, which increases the robustness of the link against interference from other nearby scatterers and fading, due to patient movements, for example. This approach also allows for simultaneous powering and communication, and inherently provides the possibility of frequency domain multiplexing to address individual nodes in implant networks. The proposed modulation scheme can be implemented in miniaturized application specific integrated circuits (ASICs), field programmable gate arrays (FPGAs), and microcontrollers, with little additional complexity. We have validated this communication scheme in a water tank setup during continuous ultrasound powering. In these experiments we achieved symbol rates of up to 100 kBd (limited in

bioRxiv preprint doi: https://doi.org/10.1101/2022.08.23.503752; this version posted August 25, 2022. The copyright holder for this preprint (which was not certified by peer review) is the author/funder, who has granted bioRxiv a license to display the preprint in perpetuity. It is made available under aCC-BY-NC 4.0 International license.

this implementation by the selected microcontroller), were able to detect the modulated signal when placing the implant transducer about 4 cm away from the focal axis and showed that this modulation scheme is more robust than OOK. This approach could provide a more stable uplink communication, particularly for miniaturized implanted devices that are located deep inside the body and need continuous ultrasonic powering.

2 Introduction

Conventional active implantable devices are powered by batteries that, when empty, need to either be replaced, or wirelessly recharged, usually inductively. Besides these conventional implants, a new family of wirelessly-powered, battery-free, active microimplants has emerged ([1], [2]). These aim to treat complex neurological disorders by providing access to various, and at times multiple, anatomical sites which can be located deep inside the body. For this scenario, ultrasonic power transfer is being investigated due to its efficiency and miniaturization advantages ([3], [4], [5], [6], [7], [8]).

Active implants often need to communicate information, for example the power status of the implant or sensor data. In conventional battery-powered active implants, Bluetooth Low Energy (BLE) is often used for communication. This provides high data rates, at the expense of comparably high power consumption. Communication then might need a large portion of the total available power. For example, in [9] the authors needed a 90 mA h battery to achieve a discharge time of up to about 12 h, with most of the power being spent for the Bluetooth system-on-chip (SoC). This translates to a power consumption of several mW. Such battery sizes and power consumption ranges are often not acceptable for miniaturized implants. For power-aware or batteryless active implants, custom wireless electromagnetic or ultrasonic communication links have been proposed. A comprehensive overview of existing methodologies for mm-sized networked implants can be found in [10] and in [11].

Electromagnetic links are widely used, however these are not suitable for miniaturized and deep implants. As explained in [10], the link frequency must be kept low to achieve low attenuation. But for low frequencies, in order to achieve sufficient coupling, the size of the coils must be at least the distance between the implanted and the external coils.

Generally, ultrasonic links have demonstrated higher penetration depths. We therefore turn to a fully-ultrasonic approach to power and communicate with deep implants. For the uplink communication of ultrasonically powered implants two approaches are generally used. The first approach, known as backscatter modulation or load modulation, exploits the bidirectional characteristics of electro-acoustic transducers. First, the implant transducer converts the incoming acoustic power into electrical power. Modulating the load connected to the transducer alters the amount of electric power which is reflected back to the transducer. The transducer, in turn, converts this reflected electrical power back into acoustic power, effectively acting as a backscatterer. An external acquisition system can pick up this backscattered signal and detect the

bioRxiv preprint doi: https://doi.org/10.1101/2022.08.23.503752; this version posted August 25, 2022. The copyright holder for this preprint (which was not certified by peer review) is the author/funder, who has granted bioRxiv a license to display the preprint in perpetuity. It is made available under aCC-BY-NC 4.0 International license.

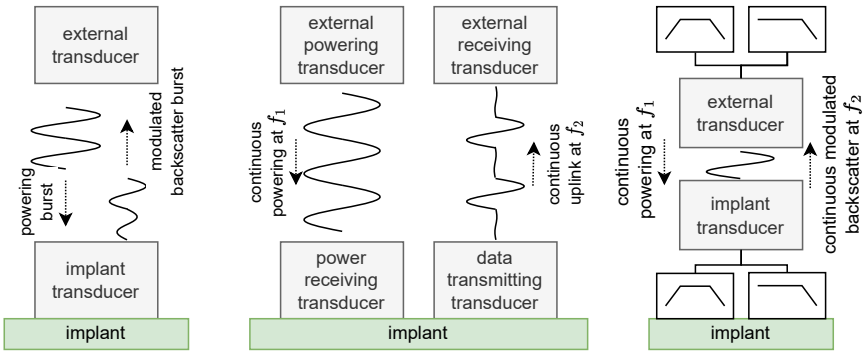

Figure 1: Available solutions for fully ultrasonic power-up and data uplinks. **left**) Backscatter modulation with time domain multiplexing: The external transducer emits a powering burst. The implant changes the electric load to its transducer, modulating the amplitude of the backscattered burst. As bursts are used, the powering of the implant is interrupted. **middle**) Dedicated transducers with frequency multiplexing: Two independent transducers are used for power transfer and uplink communication, working at different frequencies. The implant actively drives the data uplink transducer. **right**) Backscatter modulation with frequency domain multiplexing: A single transducer is used for both powering and data link. Hardware filters are used to separate the power and data link after the transducer.

changes. A more detailed explanation of this concept can be found in [12].

A second approach uses two distinct transducers, one dedicated to the power link, and an additional one for the communication uplink, as in [13] and [14]. The two links operate at different frequencies. The implant then incorporates an active circuit for driving the transducer used for communication. Such a system is described in more detail in [14].

Another approach was proposed recently in [15]. In this work, the authors combine backscattering with Frequency Division Multiplexing (FDM). With this approach, the implant transducer picks up a signal comprising two frequencies. One frequency is used for powering and another frequency for the uplink communication. The data uplink is subsequently separated from the power link via hardware filters at the implant.

A summary of these three approaches for a fully ultrasonic power-up and data uplink is schematically illustrated in Figure 1. For all approaches, variants of Amplitude Modulation (AM) [16], On-Off Keying (OOK) [14], or sometimes Pulse Width Modulation (PWM) [17] are used to encode the information.

The ultrasound backscatter modulation as a basis of OOK or AM (Figure 1-left) typically requires pulsed ultrasound [16]. Also, determining the decision boundary between the high and the low level of the backscattered ultrasound can be difficult. Recent papers mitigate this problem by measuring the difference between two consecutive pulses ([4] and [17]), at the cost of dividing the data rate by two. On the other hand, adding a second, actively driven, transducer, as in Figure 1-middle, increases the system complexity and size [16]. The same applies for the approach in [15], described in Figure 1-right, as it requires at least two additional inductors and capacitors for the filter network. These limitations become more relevant for small, low-power implants

bioRxiv preprint doi: https://doi.org/10.1101/2022.08.23.503752; this version posted August 25, 2022. The copyright holder for this preprint (which was not certified by peer review) is the author/funder, who has granted bioRxiv a license to display the preprint in perpetuity. It is made available under aCC-BY-NC 4.0 International license.

that are placed deep inside the body.

To overcome these, we propose an approach based on combining backscattering with Frequency-Shift Keying (FSK). Compared to ASK or OOK, this increases the robustness of the communication link against noise [18]. We will show that FSK is also advantageous compared to ASK when considering interference and a fading channel, for example, due to patient movements. Similar approaches have already been described for inductive links ([19], [11]). A similar approach for ultrasonic uplinks was also recently proposed in [16] by Ghanbari et al., but the subcarriers were used as a means of Code Division Multiplexing (CDM), to receive data from several implants simultaneously. Our approach would also allow for multi-device communication based on FDM or CDM, by choosing different modulation frequencies for each device. However, we only experimented with a single device. Importantly, our proposed approach allows for continuous ultrasound, using only a single transducer for power reception and communication on the implant side. Furthermore, it adds little complexity to the design of an application specific integrated circuit (ASIC) or field programmable gate arrays (FPGAs) and can also be implemented on microcontrollers.

3 Proposed modulation scheme and implementation considerations

3.1 Frequency-Shift Keying by load modulation (FSK-lm) uplink for ultrasonic biotelemetry

The proposed modulation scheme is based on the consideration that an implant needs to transfer back digital data and to be powered continuously, but the design requires a modulation scheme based on load or backscatter modulation, for example, due to size, complexity, or power constraints. In the presence of powering ultrasound, the detection of the backscattered AM signal becomes difficult, as its amplitude may be several orders of magnitude smaller than the incident ultrasound [16]. To mitigate this problem, we propose modulating the backscattered ultrasound at specific frequencies, to generate sidebands in the spectrum, which can be distinguished from the incident signal in the frequency domain. Figure 2 shows the most straightforward implementation of this concept, which is superimposing a single subcarrier onto an OOK signal.

Superimposing the subcarrier onto the OOK modulated signal simplifies the detection and decoding of the backscattered signal in the presence of a strong incident carrier, as shown in Figure 3. In the frequency domain, copies of the signal at frequencies further away from the incident ultrasound are present, providing the possibility to leverage FDM or CDM, as was done in conjunction with analog AM in [16]. It must be noted that the amplitude of these signal copies is inherently smaller compared to the amplitude of the simple OOK signal. Looking at Figure 2, one can imagine the subcarrier effectively turning off the carrier signal half of the time. This means, on average, only half of the power is transferred when OOK is combined with a rectangular subcarrier compared to simple OOK. This already reduced power is spread across the

bioRxiv preprint doi: https://doi.org/10.1101/2022.08.23.503752; this version posted August 25, 2022. The copyright holder for this preprint (which was not certified by peer review) is the author/funder, who has granted bioRxiv a license to display the preprint in perpetuity. It is made available under aCC-BY-NC 4.0 International license.

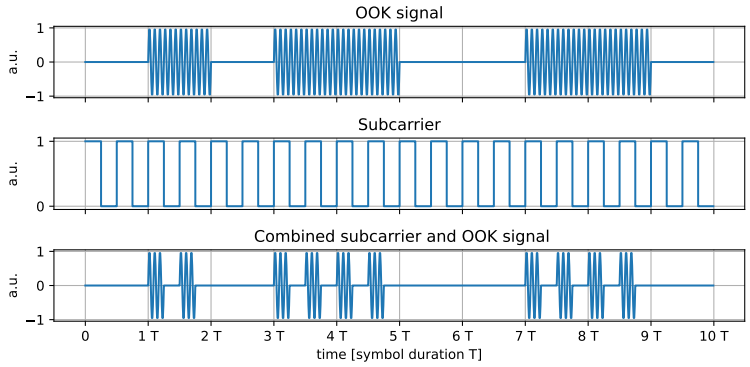

Figure 2: Comparison of simple OOK and OOK with a superimposed subcarrier. For simple OOK the carrier amplitude is kept constant during each symbol duration. The subcarrier causes several short bursts with a constant repetition rate being generated during a single symbol.

carrier and the modulation products, causing further reduction of the amplitudes in the spectrum.

Combining OOK with a subcarrier would allow for continuous ultrasound powering and simultaneous communication. However, to further simplify the detection, we used several subcarriers that are selected depending on the data, effectively behaving as FSK. In the case of two distinct frequencies, we use one frequency f_0 to encode a binary zero and another frequency f_1 to encode a binary one. This is equivalent to binary Frequency-Shift keying (BFSK). However, we do not actively drive the transducer with the two frequencies, but generate them through load modulation again. Therefore, we refer to it as Frequency-Shift Keying by load modulation (FSK-lm). Figure 4 compares this modulation scheme with OOK in the time domain.

3.2 OOK versus BFSK with multiple backscatterers

Consider a scenario as shown in Figure 5 (top). Apart from the modulating transducer, another secondary backscattering surface is located nearby (e.g. bone tissue). The backscattered bursts from the modulating transducer and nearby surface may interfere, if their distance to the external transducer is similar. This can cause bit errors in case of OOK that can be avoided with BFSK (and FSK in general). In both cases, the secondary burst suddenly changes the amplitude of the received signal compared to the modulated signal from the implant. For OOK, this invalidates the decoding levels A_0 and A_1, causing a bit error. In contrast, for BFSK a bit error can be avoided, as only the amplitudes of the superimposed modulation pulses with frequencies f_0 and f_1 are compared to each other, while the changing offset due to the secondary scattering is ignored. Considering a fading channel, where the delay of the secondary scattering fluctuates, similar difficulties exist for differential OOK or OOK during continuous ultrasound. Of course, the effects of the secondary burst cannot be completely suppressed with FSK in case it occurs somewhere in the middle of a symbol,

bioRxiv preprint doi: https://doi.org/10.1101/2022.08.23.503752; this version posted August 25, 2022. The copyright holder for this preprint (which was not certified by peer review) is the author/funder, who has granted bioRxiv a license to display the preprint in perpetuity. It is made available under aCC-BY-NC 4.0 International license.

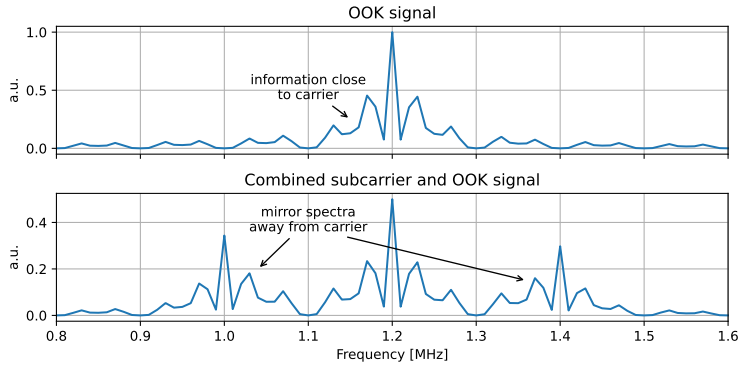

Figure 3: Comparison of a simple OOK signal with a subcarrier superimposed OOK signal in the frequency domain. For simple OOK the information of the signal is spread in the frequency content close to the carrier. This makes it susceptible to fluctuations of the carrier, that alter the frequency content around it. Superimposing the OOK signal with a subcarrier generates mirrored signals further away from the carrier, which are therefore more robust against carrier fluctuations. Due to the additional modulation, the amplitude decreases when adding subcarrier modulation.

which, in reality, is always the case. It is, nevertheless, inherently suppressed by FSK demodulation, and the robustness against this phenomenon can be adjusted by the ratio of the modulation frequencies to the symbol rate. This property becomes more important for deep implants where the received modulated signal may be comparably weak to that of scatterers closer to the external transducer.

3.3 BFSK signal generation in ASICs and microcontrollers

To generate the necessary control signal for the load switch, an ASIC or FPGA implementation would require one or more counters, depending on the specific modulation scheme (subcarrier, BFSK, or multiple Frequency-Shift Keying (MFSK)) and a few logic gates. Figure 6 shows a simplified system overview needed for binary FSK.

Alternatively, a microcontroller-based implementation could be considered, as modern µCUs are able to generate the necessary control signal for the switch. They only need a timer peripheral that generates the control signal. The modulation frequency is then changed by updating the timer's compare and period values. While many microcontrollers include timers, their capabilities differ, causing differences in the maximum possible data rate or power consumption, for example.

4 Methods

To demonstrate the feasibility of this modulation scheme, we developed a bench top prototyping platform, which uses analog switches controlled by a microcontroller. Figure 7 shows a simplified overview of that prototype.

bioRxiv preprint doi: https://doi.org/10.1101/2022.08.23.503752; this version posted August 25, 2022. The copyright holder for this preprint (which was not certified by peer review) is the author/funder, who has granted bioRxiv a license to display the preprint in perpetuity. It is made available under aCC-BY-NC 4.0 International license.

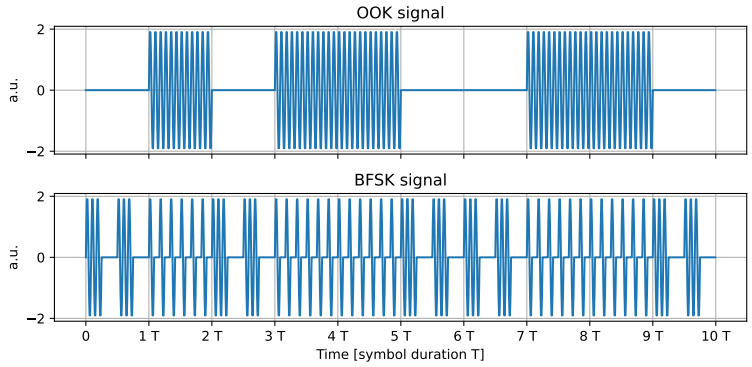

Figure 4: Comparison of OOK and BFSK by load modulation in the time domain. For OOK, the carrier is turned on depending on the value of the current bit. For BFSK, the carrier is always pulsing, only the pulse rate is changed depending on the current bit value.

We then used this prototype in two different experiments, the first investigating possible data rates and the second exploring the out-of-focus performance. Both experiments were performed in a water tank and share the same setup, shown in Figure 8.

As the external TX transducer, we used an unfocused commercial 1.27 cm submersible transducer manufactured by Olympus with a resonant frequency of 5 MHz. The external transducer was driven by a Keysight 33622A waveform generator, set to a nominal output voltage of $10\,V_{pp}$ at a $50\,\Omega$ load. For the transducer at the implant side, we used one channel of a pre-charged capacitive micromachined ultrasound transducer (CMUT)-array, described in [20]. As the CMUTs resonant frequency was measured to be close to 3.5 MHz, both experiments where performed with this carrier frequency. After measuring the electrical impedance of the transducer in water, we adapted the impedance matching network of our prototyping platform accordingly. However, as optimum power transfer was not a focus of this work, we did not optimize the impedance matching. We then placed the CMUT at a distance of approximately 11 cm on-axis of the externally driven transducer, because it gave us the maximum voltage across the CMUT. This distance is slightly larger than the theoretical focal distance of approximately 9.5 cm. The CMUT was then connected to our prototyping platform. The prototyping platform was controlled and powered via USB from a host laptop. The firmware allowed load modulation with a constant frequency, used for the out-of-focus experiment, or encoding arbitrary data with BFSK as described above, used in the data transfer experiment.

The backscattered ultrasound was picked up by a 1 mm diameter needle hydrophone from Precision Acoustics placed close to the Olympus transducer. Its output, as well as, the control signal for the analog switches, where captured with an R&S RTA4004 oscilloscope. For the data transfer experiment, we used the switching control signal as trigger for the oscilloscope, in order to easily capture the message beginning and reduce recording size. We used the 10 MHz-clock of the oscilloscope output as reference clock for the waveform generator and the prototyping platform, to keep all clocks

bioRxiv preprint doi: https://doi.org/10.1101/2022.08.23.503752; this version posted August 25, 2022. The copyright holder for this preprint (which was not certified by peer review) is the author/funder, who has granted bioRxiv a license to display the preprint in perpetuity. It is made available under aCC-BY-NC 4.0 International license.

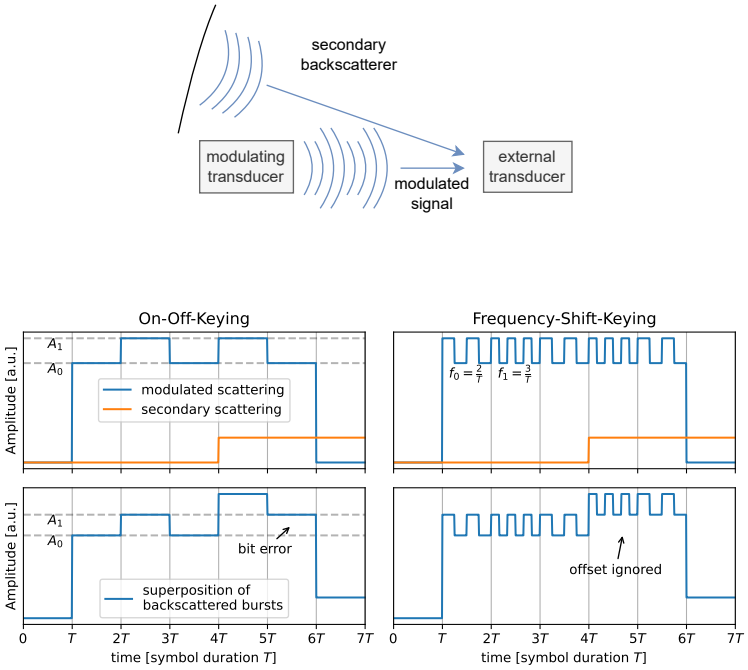

Figure 5: top) Model to compare ASK/PWM with FSK in the presence of a second backscattering surface. Depending on the distances of the modulating transducer and the secondary backscatterer to the external transducer, the backscattered bursts can interfere. Due to patient movements, for example, the interference may change over time. **bottom**) Simplified simulation of the amplitude of backscattered signals for OOK and BFSK in the presence of a secondary scatterer. While the secondary burst introduces a bit error at the receiver for OOK, the introduced amplitude change is ignored as offset in case of FSK demodulation.

synchronized.

For the data transfer experiment, the CMUT was kept at the same position, but we increased the symbol rate from 1 kBd to 100 kBd. We also increased the encoding frequencies accordingly to at least two times the symbol rate, with the highest switching frequency reaching 400 kHz. For the out-of-focus experiment, we chose a fixed modulation frequency of 200 kHz and moved the CMUT to the side for 4 cm in 1 mm steps. To be precise, the hydrophone and TX transducer were slightly tilted inwards, so their center axes formed an isosceles triangle pointing towards the CMUT. Thus, the movement of the CMUT was not exactly perpendicular to the TX transducer's focal axis. However, measuring the angles and distances of the setup was not possible. At each step, we recorded the hydrophone signal for 1.2 ms, corresponding to a symbol rate of 833 Bd, for offline analysis.

bioRxiv preprint doi: https://doi.org/10.1101/2022.08.23.503752; this version posted August 25, 2022. The copyright holder for this preprint (which was not certified by peer review) is the author/funder, who has granted bioRxiv a license to display the preprint in perpetuity. It is made available under aCC-BY-NC 4.0 International license.

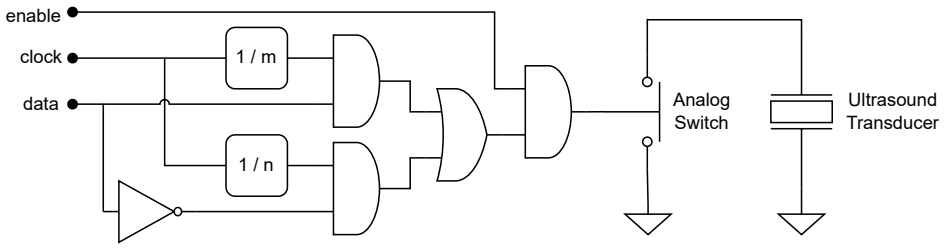

Figure 6: Simplified overview of the components needed to get a BFSK signal by load modulation. A clock signal is fed to two clock dividers, using integer denominators m and n with $m \neq n$ and generating the necessary modulation frequencies. The input signal "data" is a binary data stream. The logic gates select the modulation frequency depending on the bit value in the data stream. The symbol time of the data stream must be an integer multiple of the two modulation periods. The enable signal is optional and might alternatively shut off the whole circuit, when no communication is needed.

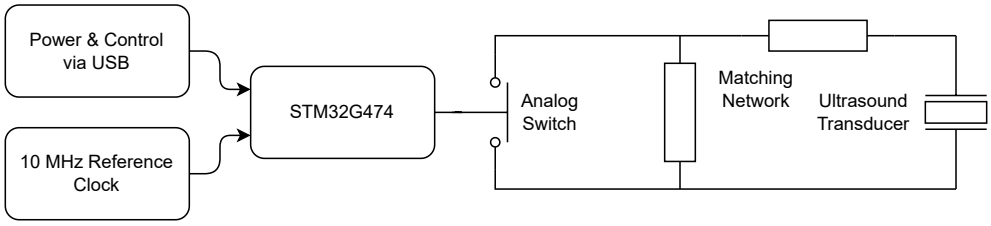

Figure 7: Simplified system overview of the prototyping platform based on the STM32G474 microcontroller and ADG1401 analog switch.

5 Results

5.1 Data transfer rate

For the data transfer experiment, we achieved symbol rates of up to 100 kBd, as shown in Figure 9. At that symbol rate, the microcontroller started not being able to update the switching frequency for the next symbol in time. Otherwise, the bandwidth and noise of the channel would have allowed for higher symbol rates.

5.2 Out-of-focus performance

For the out-of-focus experiment, an initial 60 µs burst was sent, which allowed us to estimate the distances and how the ultrasound waves propagate with the CMUT on-axis. Figure 10 shows the recorded signals of this burst.

After about 80 µs, the burst reached the CMUT and after about another 80 µs, the hydrophone picked up the backscattered and modulated burst. For the voltage at the CMUT, one can see a periodic disturbance, also without the ultrasound burst being present. This is caused by the parasitic input capacitance of the analog switches MOS-

bioRxiv preprint doi: https://doi.org/10.1101/2022.08.23.503752; this version posted August 25, 2022. The copyright holder for this preprint (which was not certified by peer review) is the author/funder, who has granted bioRxiv a license to display the preprint in perpetuity. It is made available under aCC-BY-NC 4.0 International license.

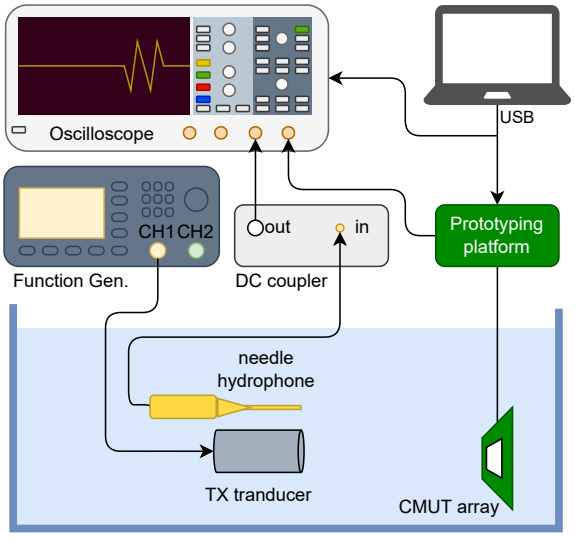

Figure 8: Setup of the performed experiments. The synchronization of the function generator and the prototyping platform to reference clock output of the oscilloscope is not shown.

FETs, which results in brief current spikes flowing through the CMUT whenever the analog switches state is changed. To ensure that we did not accidentally misinterpret the ultrasound pulses generated by this disturbance as our modulation signal, we chose the modulation frequency in a way that the frequencies of the modulation products would not be harmonics of the modulation frequency itself. With a carrier frequency of $f_c = 3.5\,\mathrm{MHz}$, the closest modulation products become $f_c - f_{mod} = 3.3\,\mathrm{MHz}$ and $f_c + f_{mod} = 3.7\,\mathrm{MHz}$. As these frequencies are not integral multiples of the modulation frequency f_{mod}, we can be sure that we did not detect a harmonic of these pulses.

Then we moved the CMUT in 1 mm steps laterally out of the focal axis of the TX transducer. For each step, the CMUT and hydrophone signal were recorded for 1.2 ms, equivalent to a symbol rate of approximately 833 Bd. We extracted the modulation products from the hydrophone signal for each step using an FFT. Figure 11 plots the calculated amplitudes at the CMUT and the hydrophone depending on the position of the CMUT.

The figure shows that in our setup the amplitude of the modulation products remains 10 dB above the noise floor, with the CMUT array up to 4 cm away from the optimum position. The only exception is at 32 mm, where the received acoustic power at the CMUT drops by several orders of magnitude. We estimated the noise floor from the measured amplitude at frequencies away from the carrier and the modulation products.

bioRxiv preprint doi: https://doi.org/10.1101/2022.08.23.503752; this version posted August 25, 2022. The copyright holder for this preprint (which was not certified by peer review) is the author/funder, who has granted bioRxiv a license to display the preprint in perpetuity. It is made available under aCC-BY-NC 4.0 International license.

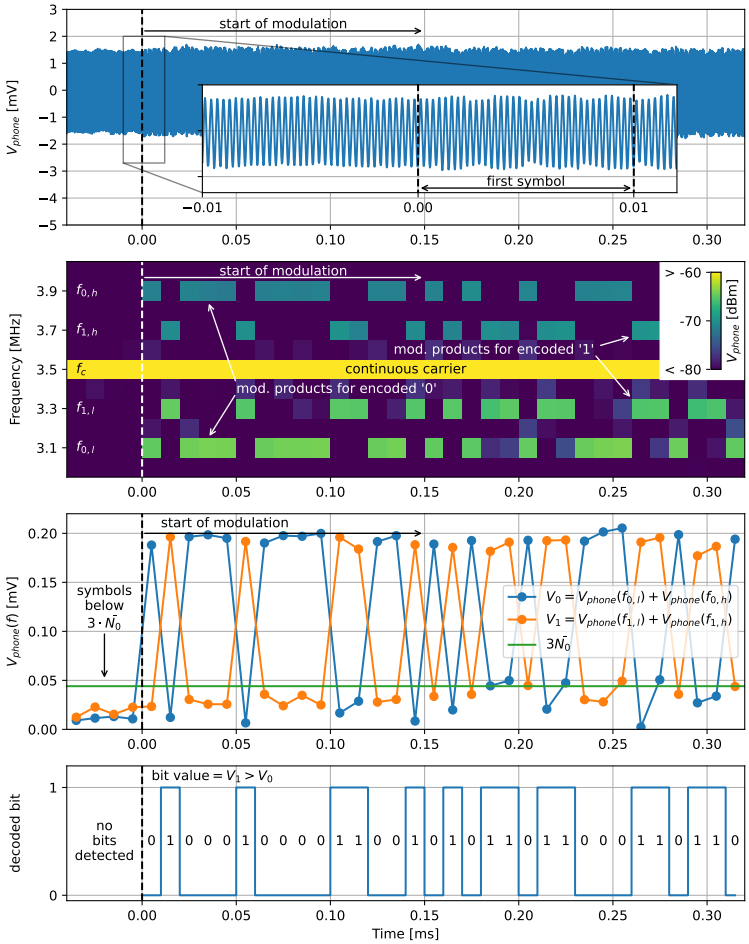

Figure 9: Decoding of the recorded signal for a symbol rate of 100 kB. Zeros are encoded with a modulation frequency of $f_0 = 400\,\text{kHz}$, ones with $f_1 = 200\,\text{kHz}$. **top**) captured hydrophone signal showing the beginning of the modulation at $t = 0\,\text{ms}$. **middle top**) Spectrogram of the backscattered signal. From $t = 0\,\text{ms}$ on, the modulation products above and below the carrier frequency are visible. The signal range was compressed to visually enhance the modulation products at $f_{0,l} = 3.1\,\text{MHz}$, $f_{1,l} = 3.3\,\text{MHz}$, $f_{1,h} = 3.7\,\text{MHz}$ and $f_{0,h} = 3.9\,\text{MHz}$. **middle bottom**) Measured amplitude of the modulation products. The respective mean of the upper and lower modulation products is plotted. During the first four symbols, no modulation happens. From these, the estimated system noise $\bar{N}_0$ is calculated. **bottom**) The demodulated and decoded binary data.

bioRxiv preprint doi: https://doi.org/10.1101/2022.08.23.503752; this version posted August 25, 2022. The copyright holder for this preprint (which was not certified by peer review) is the author/funder, who has granted bioRxiv a license to display the preprint in perpetuity. It is made available under aCC-BY-NC 4.0 International license.

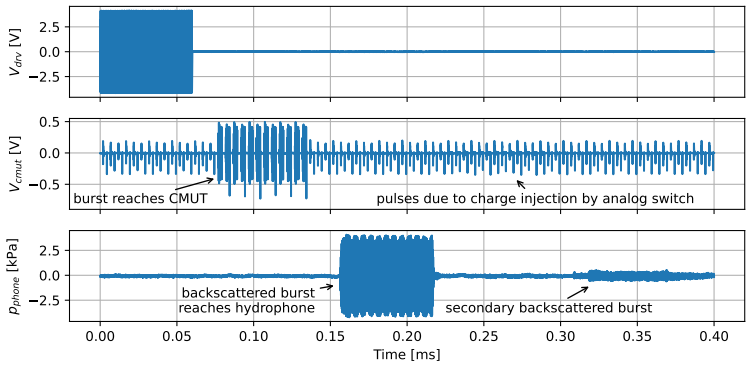

Figure 10: Burst to measure distances at the start position of the out-of-focus scan. **top**) The driving voltage of the external transducer reaches about 8 V_{pp}. **mid**) After about 0.8 ms the burst reaches the CMUT. Before and after the burst, a continuous disturbance in the form of pulses is visible. These pulses are caused by the charge injection of the internal MOSFETs in the analog switch. From these, the modulation frequency (here 200 kHz) can be verified. **bottom**) After approximately another 0.8 ms, the backscattered burst reaches the hydrophone with visible modulation. After about 0.32 ms, secondary backscattered bursts are reaching the hydrophone. These could interfere with the modulated signal for consecutive pulses and harm the decoding when using ASK.

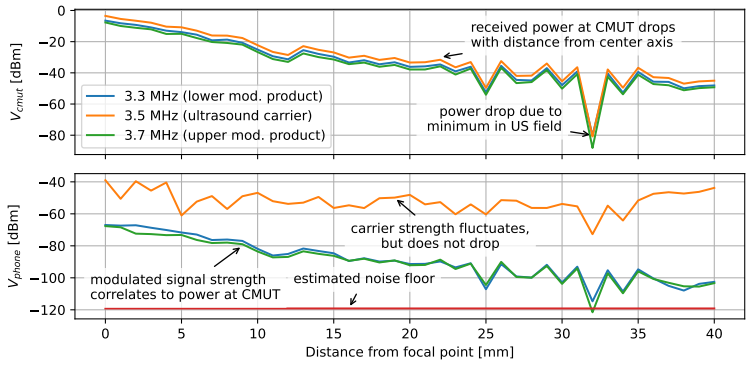

Figure 11: Measured signal strengths depending on the CMUT transducer's distance to the TX transducer's focal axis. **top**) Voltage across the CMUT transducer that modulates the ultrasound. As the modulation switch is shorting the CMUT, the modulation depth is close to 100 %, and the amplitude of the modulation products is close to the carrier amplitude. At a distance of 32 mm, the ultrasound field has a local minimum. Therefore, the amplitude drops by about two orders of magnitude. **bottom**) The backscattered signal, picked up by the hydrophone. While the amplitude of the modulation products has a visible correlation to their amplitude at the CMUT transducer, the carrier amplitude is mostly dependent on the backscattering of the surrounding setup i.e. walls of the water tank and mounting posts. The grey line at the bottom of the graph is the noise floor of the acquisition system estimated from the mean of the measured values at 3.65 MHz. With the exception at 32 mm, the received modulation products stay about 10 dB or more above this noise floor.

bioRxiv preprint doi: https://doi.org/10.1101/2022.08.23.503752; this version posted August 25, 2022. The copyright holder for this preprint (which was not certified by peer review) is the author/funder, who has granted bioRxiv a license to display the preprint in perpetuity. It is made available under aCC-BY-NC 4.0 International license.

6 Discussion

In this study, we have proposed Frequency-Shift Keying by load modulation for ultrasonic uplink communication from small and deep implants. Our proposed approach, as opposed to time-multiplexed schemes as in Figure 1-left, allows ultrasonic communication with uninterrupted power transfer, thus maximizing the amount of power that can reach the implant. In contrast to [16], the additional subcarrier is not used to differentiate between several implants, but instead to differentiate the backscattered signal from the incident ultrasound. Our approach would also allow for multi-device communication based on FDM, by choosing different frequencies for each device, but at the expense of lower data rates. A similar modulation approach, using a single subcarrier, is standardized for inductive Near-Field Communication (NFC) of identification/proximity cards in ISO/IEC 14443-2 [1] . However, NFC is unsuitable for deep implant uplink communication, due to attenuation and insufficient coupling issues, as described above. Furthermore, the standard does not support multiple access scenarios.

The frequency of the powering ultrasound, depends on the geometry of the ultrasound link and the transducers in use. Thus, finding the optimum modulation frequencies for FSK and symbol rate is a challenge, that has to be uniquely solved for each system or use case. In theory, in this scheme, the subcarrier frequency can be adapted on the fly. However, for FPGA/ASIC implementations this would add to the circuit complexity and the adaption algorithms will have to be developed and adapted for different systems.

The experimental validation of this scheme comes with some practical limitations, which are discussed below.

The proposed communication scheme has been validated using a benchtop setup, and practical choices related to this validation, such as the equipment used, will unavoidably affect and often determine the measured experimental performance.

For example, in this study we have demonstrated symbol rates of up to 100 kBd. This symbol rate can be limited by the bandwidth of the transducer or the impedance matching network. The spectrogram in Figure 9 shows that the amplitude of the upper modulation products is a few dB below that of the lower modulation products. The reason is that the pass band of the transducer or the matching network is not centered or symmetric around the carrier frequency and the upper frequencies are attenuated more. A higher symbol rate would have required even higher modulation frequencies, causing more and more attenuation, and, at some point the modulation products would not be detectable anymore. In case of an implementation where PZT transducers were chosen instead, the maximum possible data rate might also be reduced, since their bandwidth is typically smaller than that of CMUTs. Further optimizing the matching network might have decreased the bandwidth as well, and so the modulation depth and Signal-to-Noise Ratio (SNR).

The SNR depends on the inherent noise of the acquisition system. Choosing another

[1] It is also combined with Manchester coding, which simplifies clock synchronization. To keep the system simple, we did not add Manchester coding so far.

bioRxiv preprint doi: https://doi.org/10.1101/2022.08.23.503752; this version posted August 25, 2022. The copyright holder for this preprint (which was not certified by peer review) is the author/funder, who has granted bioRxiv a license to display the preprint in perpetuity. It is made available under aCC-BY-NC 4.0 International license.

hydrophone or oscilloscope, therefore would have changed the system performance. The SNR also decreases when increasing the symbol rate. Increasing the distance will lead to lower SNR as well. In our case, with a symbol rate of 100 kBd and a distance of 11 cm, we achieved a SNR of approximately 20 dB. So, depending on the required SNR, higher symbol rates and distances are possible.

In this implementation, the main limiting factor for the symbol rate was the time the microcontroller needed to update its timer peripheral for the next symbol. Increasing its core clock frequency, using a faster microcontroller, or leveraging direct memory access techniques would have allowed for higher data rates.

Other studies with a focus on millimeter scale implants have reported data rates of 40 kbit s^{-1} ([10] and [14]), 95 kbit s^{-1} with dedicated transducers for the data uplink [13], and a possible 200 kbit s^{-1} in [15], derived from the pulse response of the system. In [4], the symbol rate is in the order of 1 kBd, but depends mainly on the pulse repetition rate. If size and implant depth are of no concern, ultrasound communication is capable of achieving data rates in the range of 100 Mbit s^{-1} ([21] and [22]). We expect our scheme to also be capable of reaching several Mbit s^{-1} in an experimental setup, if optimized for maximum data rate, ignoring other constraints, such as power, size, complexity, depth, etc. However, in this case, using other modulation schemes could be more advantageous as they would allow for even higher data rates and better robustness, as has been done in [21] and [22]. Overall, for similar scenarios comparable rates to the literature are achievable with our approach.

However, the focus of our approach is not high data rates but the relatively high robustness combined with minimum added complexity and versatility (e.g. suitable to be implemented on virtually any microcontroller). To demonstrate this robustness, we have considered a scenario where out-of-focus detection is required.

We were not able to find any relevant reports on the out-of-focus detection performance in the literature. We assume the reason for that is that perfect alignment is necessary/implied for systems benchmarked so far. However, out-of-focus performance might be essential to retain a stable communication link in case of sudden movements, for example. The experiment shows that for the given setup the SNR remains above 10 dB for distances up to 4 cm, as long as the receiving transducer is not located at a local minimum of the incident ultrasound field. According to [23], the bit error probability for noncoherent BFSK in this case remains well below 10 % and can be as low as 0.1 %, depending on the channel's fading properties. Higher out-of-focus distances are likely possible, but our setup geometry did not allow moving further.

Comparing the robustness of our scheme to that achieved by OOK/ASK modulation, we can see that the main advantage of our approach can be derived from the ratio between the received modulation amplitude and the fluctuations of the carrier amplitude. This ratio can reach several orders of magnitude. In our experiment, for example, when moving from 27 mm to 28 mm, the carrier backscattered from the surrounding changes by about 230 µV. However, the modulation changes the backscattered amplitude by only approximately 2.3 µV at 28 mm. For OOK, the high ratio makes it difficult for the decoding algorithms to let the decision boundary track the carrier fluctuations. FSK, on the other hand, is more robust against amplitude fluctuations, because the demodulation algorithm suppresses them.

bioRxiv preprint doi: https://doi.org/10.1101/2022.08.23.503752; this version posted August 25, 2022. The copyright holder for this preprint (which was not certified by peer review) is the author/funder, who has granted bioRxiv a license to display the preprint in perpetuity. It is made available under aCC-BY-NC 4.0 International license.

As an additional remark, it should be noted that all experiments were performed in a water tank, i.e. in a very controlled environment. For example, in a real world scenario, the medium would be tissue instead of water, which has higher attenuation. We could also expect larger misalignment and scattering from other surfaces or implants. This could reduce the SNR, which means the distances or data rates achieved in this experiment might not be feasible. However, the outlined advantages over OOK should apply in just these scenarios.

Finally, in the current implementation, all signals were recorded using an oscilloscope and analyzed offline later. Future work will have to show online decoding to reduce saved data size and allow for closed loop systems. In addition, the performance of other modulation schemes like MFSK, Phase-Shift Keying (PSK), or Quadrature Amplitude Modulation (QAM) can possibly be implemented with our prototyping platform and may improve performance. For example in [18], binary Phase-Shift Keying (BPSK) is shown to have a lower bit error rate (BER) than BFSK. Adding Manchester coding could simplify the clock synchronization. A future version of the prototyping platform could be powered from the ultrasound carrier itself, to show the feasibility of combining both links.

7 Conclusion

In this work, we have proposed a data communication scheme based on Frequency-Shift Keying by load modulation (FSK-lm), to enable robust ultrasonic uplink communication during continuous ultrasonic power transfer in small and deep implants. A unique transducer on the implant side is sufficient for simultaneous power reception and communication. Our experiments showed that FSK-lm, compared to the more common OOK/ASK approaches in ultrasonic uplinks, increases the communication robustness, while achieving similar symbol rates. We used an off-the-shelf microcontroller to generate the necessary control signal for the load modulation switch and showed that integration into an ASIC requires only a few additional circuits.

Acknowledgements

This work is part of the Moore4Medical project funded by the ECSEL Joint Undertaking under grant number H2020-ECSEL-2019-IA-876190.

References

[1] Vasiliki Giagka and Wouter A. Serdijn. "Realizing flexible bioelectronic medicines for accessing the peripheral nerves – technology considerations." In: *Bioelectronic Medicine* 4.1 (June 2018), p. 8. ISSN: 2332-8886. DOI: 10.1186/s42234-018-0010-y.

bioRxiv preprint doi: https://doi.org/10.1101/2022.08.23.503752; this version posted August 25, 2022. The copyright holder for this preprint (which was not certified by peer review) is the author/funder, who has granted bioRxiv a license to display the preprint in perpetuity. It is made available under aCC-BY-NC 4.0 International license.

[2] Yan Liu et al. "Bidirectional bioelectronic interfaces: System design and circuit implications." In: *IEEE Solid-State Circuits Magazine* 12.2 (2020), pp. 30–46. DOI: 10.1109/MSSC.2020.2987506.

[3] Lucia Tacchetti, Wouter A. Serdijn, and Vasiliki Giagka. "An Ultrasonically Powered and Controlled Ultra-High-Frequency Biphasic Electrical Neurostimulator." In: *2018 IEEE Biomedical Circuits and Systems Conference (BioCAS)*. Oct. 2018, pp. 1–4. DOI: 10.1109/BIOCAS.2018.8584718.

[4] David K. Piech et al. "A wireless millimetre-scale implantable neural stimulator with ultrasonically powered bidirectional communication." In: *Nature Biomedical Engineering* 4.2 (2020), pp. 207–222. DOI: 10.1038/s41551-020-0518-9.

[5] Patrick J. Larson and Bruce C. Towe. "Miniature ultrasonically powered wireless nerve cuff stimulator." In: *2011 5th International IEEE/EMBS Conference on Neural Engineering*. IEEE, 2011, pp. 265–268. DOI: 10.1109/NER.2011.5910538.

[6] Jayant Charthad et al. "A mm-sized wireless implantable device for electrical stimulation of peripheral nerves." In: *IEEE transactions on biomedical circuits and systems* 12.2 (2018), pp. 257–270. DOI: 10.1109/TBCAS.2018.2799623.

[7] Amin Rashidi et al. "An implantable ultrasonically powered system for optogenetic stimulation with power-efficient active rectifier and charge-reuse capability." In: *IEEE Transactions on Biomedical Circuits and Systems* 13.6 (2019), pp. 1362–1371. DOI: 10.1109/TBCAS.2019.2949154.

[8] Dongjin Seo et al. "Wireless recording in the peripheral nervous system with ultrasonic neural dust." In: *Neuron* 91.3 (2016), pp. 529–539. DOI: 10.1016/j.neuron.2016.06.034.

[9] Choong Yeon Kim et al. "Soft subdermal implant capable of wireless battery charging and programmable controls for applications in optogenetics." en. In: *Nature Communications* 12.1 (Dec. 2021), p. 535. ISSN: 2041-1723. DOI: 10.1038/s41467-020-20803-y.

[10] Max L. Wang et al. "Wireless data links for next-generation networked microimplantables." In: *2018 IEEE Custom Integrated Circuits Conference (CICC)*. Apr. 2018, pp. 1–9. DOI: 10.1109/CICC.2018.8357096.

[11] Virgilio Valente. "Evolution of Biotelemetry in Medical Devices: From Radio Pills to mm-Scale Implants." en. In: *IEEE Transactions on Biomedical Circuits and Systems* (2022), pp. 1–21. ISSN: 1932-4545, 1940-9990. DOI: 10.1109/TBCAS.2022.3190767.

[12] Mohammad Meraj Ghanbari and Rikky Muller. "Optimizing Volumetric Efficiency and Backscatter Communication in Biosensing Ultrasonic Implants." In: *IEEE Transactions on Biomedical Circuits and Systems* 14.6 (Dec. 2020), pp. 1381–1392. ISSN: 1940-9990. DOI: 10.1109/TBCAS.2020.3033488.

[13] Ting Chia Chang et al. "27.7 A 30.5 mm 3 fully packaged implantable device with duplex ultrasonic data and power links achieving 95kb/s with< 10- 4 BER at 8.5 cm depth." In: *2017 IEEE International Solid-State Circuits Conference (ISSCC)*. IEEE, 2017, pp. 460–461. DOI: 10.1109/ISSCC.2017.7870460.

bioRxiv preprint doi: https://doi.org/10.1101/2022.08.23.503752; this version posted August 25, 2022. The copyright holder for this preprint (which was not certified by peer review) is the author/funder, who has granted bioRxiv a license to display the preprint in perpetuity. It is made available under aCC-BY-NC 4.0 International license.

[14] Marcus J. Weber et al. "A high-precision 36 mm3 programmable implantable pressure sensor with fully ultrasonic power-up and data link." In: *2017 Symposium on VLSI Circuits*. June 2017, pp. C104–C105. DOI: 10.23919/VLSIC.2017.8008564.

[15] Ahmed Allam, Karim Sabra, and Alper Erturk. "Piezoelectric transducer design for simultaneous ultrasonic power transfer and backscatter communication." en. In: *Smart Materials and Structures* 31.9 (July 2022), p. 095003. ISSN: 0964-1726. DOI: 10.1088/1361-665X/ac7b57.

[16] Mohammad Meraj Ghanbari et al. "A sub-mm 3 ultrasonic free-floating implant for multi-mote neural recording." In: *IEEE Journal of Solid-State Circuits* 54.11 (2019), pp. 3017–3030. DOI: 10.1109/JSSC.2019.2936303.

[17] Shinnosuke Kawasaki et al. "A microwatt telemetry protocol for targeting deep implants." In: *2021 IEEE International Ultrasonics Symposium (IUS)*. IEEE, 2021, pp. 1–4. DOI: 10.1109/IUS52206.2021.9593603.

[18] Marco Privitera, Andrea Ballo, and Alfio Dario Grasso. "A 0.63 pJ/bit Fully-Digital BPSK Demodulator for US-powered IMDs downlink in a 28-nm bulk CMOS technology." In: *2022 17th Conference on Ph.D Research in Microelectronics and Electronics (PRIME)*. June 2022, pp. 125–128. DOI: 10.1109/PRIME55000.2022.9816752.

[19] Vincent W. Leung et al. "A CMOS distributed sensor system for high-density wireless neural implants for brain-machine interfaces." In: *ESSCIRC 2018-IEEE 44th European Solid State Circuits Conference (ESSCIRC)*. IEEE, 2018, pp. 230–233. DOI: 10.1109/ESSCIRC.2018.8494335.

[20] Shinnosuke Kawasaki et al. "Pre-charged collapse-mode capacitive micromachined ultrasonic transducer (CMUT) for broadband ultrasound power transfer." In: *2021 IEEE Wireless Power Transfer Conference (WPTC)*. IEEE, 2021, pp. 1–4. DOI: 10.1109/WPTC51349.2021.9458104.

[21] Thomas Riedl and Andrew Singer. "Towards a video-capable wireless underwater modem: Doppler tolerant broadband acoustic communication." In: *2014 Underwater Communications and Networking (UComms)*. IEEE, 2014, pp. 1–5. DOI: 10.1109/UComms.2014.7017122.

[22] Andrew Singer, Michael Oelze, and Anthony Podkowa. "Mbps experimental acoustic through-tissue communications: MEAT-COMMS." In: *2016 IEEE 17th International Workshop on Signal Processing Advances in Wireless Communications (SPAWC)*. IEEE, 2016, pp. 1–4. DOI: 10.1109/SPAWC.2016.7536815.

[23] Marvin K. Simon and M.-S. Alouini. "Average bit error probability performance for optimum diversity combining of noncoherent FSK over Rayleigh fading channels." In: *IEEE International Conference on Communications, 2003. ICC'03.* Vol. 4. IEEE, 2003, pp. 2768–2772. DOI: 10.1109/ICC.2003.1204496.